Low-frequency nonreciprocal flexural wave propagation via compact cascaded time-modulated resonators

Sheng Wan, Liyun Cao, Yi Zeng, Tong Guo, Mourad Oudich, Badreddine Assouar

Low-frequency nonreciprocal flexural wave propagation via compact cascaded time-modulated resonators

Sheng Wan[1], Liyun Cao[1], Yi Zeng[1], Tong Guo[1], Mourad Oudich[1,2,*], Badreddine Assouar[1, †]

[1]*Université de Lorraine, CNRS, Institut Jean Lamour, 54000 Nancy, France*

[2]*Graduate Program in Acoustics, The Pennsylvania State University, University Park, Pennsylvania 16802, USA*

Corresponding authors

[*]mourad.oudich@univ-lorraine.fr

[†]badreddine.assouar@univ-lorraine.fr

Keywords: Nonreciprocal acoustics; Elastic metamaterials; Unidirectional wave propagation; Flexural waves

Abstract

Nonreciprocal mechanical devices are of great interest for directional elastic wave manipulation. In this letter, we introduce a design of a compact low-frequency nonreciprocal metamaterial for flexural waves, whose dimension is less than $1/3$ of the operating wavelength. This structure is made of two well-placed coil-cantilever-magnet resonators where the electromagnetic forces can be temporally modulated, which enables time varying of the effective stiffness of the resonators. A phase shift is introduced between the stiffness modulations of these two resonators which breaks the time-reversal symmetry and enables nonreciprocal wave propagation at the resonance frequency of the structure. A semi-analytical method based on harmonic waves decomposition is developed to describe the system, leading to results that match well with the numerical predictions from finite element method. We also experimentally demonstrate nonreciprocal flexural wave propagation with good agreement with the predictions made. Our system could inspire the design of compact nonreciprocal devices for flexural waves.

Breaking reciprocity in classical waves has been gaining increasing interest in the last decade, motivated by the need for unidirectional wave propagation and robust one-way waveguding[1–5]. Nonreciprocal materials or devices, i.e., diodes, are highly desired for the manipulation of the energy carried by the wave. In acoustics, a popular approach to realize nonreciprocal wave propagation by breaking the time reversal symmetry is the realization of acoustic circulators[6–8] which is inspired from optical ones[9,10]. The circulator is a three-port system with a central ring cavity endowed with a circulating fluid flow to introduce the acoustic bias[6]. Another mainstream approach is modulated phononic crystals and metamaterials[1]. This idea can be traced back to last mid-century in photonics and electrical circuits, where permittivity, permeability or the electrical impedance is harmonically modulated both in space and time to create unidirectional band gaps for waves[11–13]. The spatiotemporal modulation can also break the time reversal symmetry, leading to asymmetrical frequency conversions in opposite propagating directions. In elastodynamics, the spatiotemporal modulation is performed over the intrinsic properties of the material, namely the effective stiffness, using exotic physical and technical approaches. For the achievement of nonreciprocity for elastic waves, the challenge was to come up with a realizable method that can enable dynamic modulation of the stiffness with speed comparable to the propagating wave velocity. Wang *et al.*[14] were the first to experimentally perform such modulation using coupled magnet rings and coils where the coupling can be varied in time via dynamically changing the magnetic force from the coils which in turn leads to the time modulation of the effective stiffness. The system is equivalent to a series of masses and springs connected to the ground where the effective stiffness of the springs is modulated both in space and time. This magnet-coil based approach was proven to be very effective for modulating the effective stiffness in time at high speed which enables nonreciprocal wave dispersion. Chen *et al.*[15] designed a tunable elastic metamaterial made of periodic resonators distributed on a plate. Each resonator is constructed with a permanent magnet and a coil to control its effective stiffness, which led to a demonstration of unidirectional propagation of flexural waves. Another interesting yet different approach was proposed by Goldsberry *et al.*[16] who used nonlinear large deformations to spatiotemporally vary the effective stiffness and enable nonreciprocal wave propagation. Differently, Ruzzene *et al* [17–19] proposed an efficient and fast approach to demonstrate nonreciprocal reflection and transmission of flexural waves. In their case, the modulation of the effective stiffness is performed using piezoelectric patches connected to well elaborated and controlled electrical circuits. Besides, a mechanical approach was introduced by Attarzadeh *et al.*[20]. They used a series of local resonators where their effective stiffness was modulated by varying the second

area moment of inertia of each resonator's arm through dynamically changing its angular orientation. However, these experimental works rely on using several periods of the phononic crystal or the metamaterial in order to introduce a waveform variation of the effective stiffness both in space and time. This makes the design cumbersome and hard to be considered for subwavelength applications where compact and integrated designs with high performance wave functionalities are desired. Furthermore, in these proposed designs, a programmable micro-controller unit (MCU) is needed to synchronize the temporal modulation which seriously complicates the system. Nevertheless, promising solutions for enabling nonreciprocity using compact devices were proposed in acoustics which are based on only two cascaded local resonators. These include slab resonators[21], Helmholtz resonators[22], air cavity resonators[23], and thin membranes[24]. The compactness of those structures makes them to be of great usability for miniaturized acoustic devices.

In this research, we designed and fabricated a compact low-frequency nonreciprocal waveguide for flexural waves using only two time-modulated mechanical resonators. Inspired by the work of Chen *et al*[15] and Wang *et al.*[14], the resonators are physically realized by a coil-cantilever-magnet system with controllable effective stiffness via the application of an alternating current (AC). These resonators can be modeled as spring-mass equivalent system with time-dependent effective stiffness. By introducing a phase shift between the applied alternating current (AC) of these two resonators, their effective stiffness is harmonically modulated in time with a controllable phase shift which provokes a spatial bias, and leads to nonreciprocal flexural wave transmission. A simplified analytic approach based on plane wave decomposition is developed to analyze the flexural wave propagation in the system. The analytical results support the observed experiment ones around the adopted operating frequency. The dimension of the cascaded resonator structure is less than 1/3 of the operating wavelength.

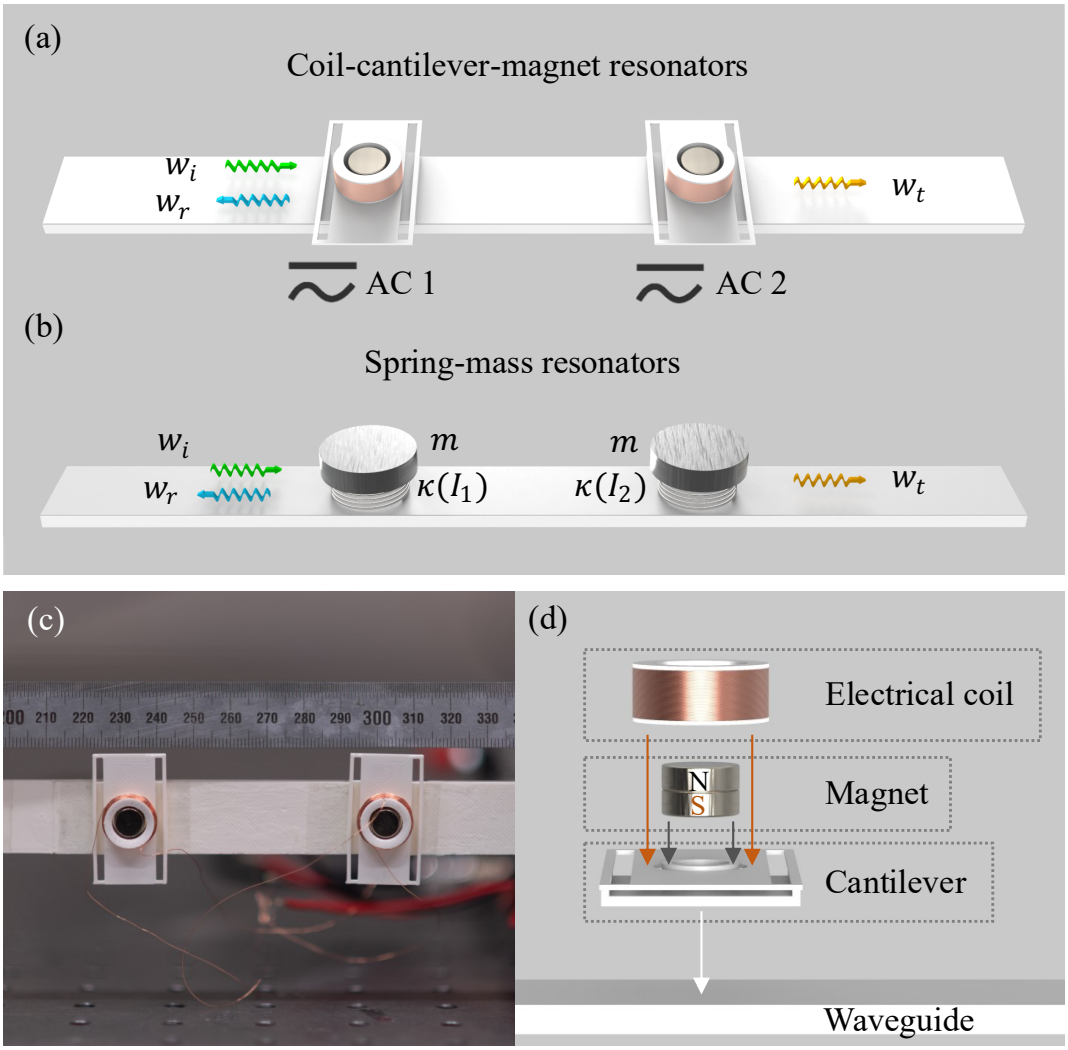

FIG. 1. (a) Realization of a coil-cantilever-magnet bi-resonator system with temporally modulated effective stiffness through an applied AC in the coil. (b) Schematic of the equivalent model for the cascaded mass-spring resonator system. AC is the alternating current, m is mass of the resonator, κ is its stiffness, I is the real-time current, w_i is the incident wave, w_r is reflected wave, and w_t is transmitted wave. (c) Fabricated on-beam coil-cantilever-magnet resonator in our experimental setup. (d) Schematic design of the coil-cantilever-magnet resonator system.

We begin by conducting a theoretical study where we model our system by the equivalent cascaded mass-spring resonator system shown in **Fig. 1(b)**. The thickness of the beam waveguide denotes h, and its width denotes d. Two mass-spring resonators are attached to the beam, whose mass is denoted m, and the time-varying spring stiffness is κ. The distance between the centers of the two resonators is l. The damping is not considered in this theoretical study. **Fig. 1(a)** shows the physical realization of this system where the resonator is made of a flexible cantilever in which a permanent magnet is fixed to the base of cantilever, and a coil is fixed to the flexible part of cantilever (**Fig.1(d)**). **Fig. 1(c)** shows the fabricated sample with

the two coil-cantilever-magnet resonators system. When no temporal modulation is applied, the coil-cantilever-magnet resonator behaves as a simple mass-spring resonator with constant mechanical properties. On the first resonance mode of the coil-cantilever-magnet structure, the displacement of the coil is only out-of-plane (see **Supplementary information**), the cantilever and the coil can be considered as the spring and the mass respectively. When the displacement of the coil is relatively small, the out-of-plane force on the coil has a linear relationship with the displacement, respecting the Hooke's law. The equivalent effective spring stiffness and mass can be evaluated via eigenfrequency study by numerical simulation using finite element method. We used the commercial software COMSOL Multiphysics 5.6 to perform such simulation (see **Supplementary information**). As for the temporal modulation, it is realized via the electromagnetic force between the coil and the magnet. When applying an AC to the coil, an attraction or repulsion force, depending on the current direction and magnetic pole orientation of magnet, appears between the magnet and the coil. This force has a linear correlation with the relative displacement between the magnet and the coil when the displacement amplitude is relatively small[15] (see **Supplementary information**). So, an additional stiffness, which could be positive or negative, is provided by the magnet-coil design and can be linearly superposed with the static stiffness of the coil-cantilever structure. Consequently, we can dynamically change the total stiffness by varying the AC applied to the coil.

To theoretically characterize the wave propagation in this system, we have considered the mass-spring model with variable effective stiffness of the springs. The out-of-plane displacement fields of the incident, reflected, and transmitted waves are denoted as w_i, w_r, and w_t (**Fig. 1(a)** and **(b)**). In the one-dimensional theoretical model, the plate model is adopted, and the dimensions of the resonator are not considered. We first start with a system with only one resonator located at $x = 0$. The temporal modulation on the spring stiffness of the form $\kappa(t) = \kappa_0 + \kappa_m \cos(\Omega t + \phi)$ is considered where Ω is the modulation frequency, ϕ is the initial phase, κ_0 is the static spring stiffness associated with the flexible cantilever, and κ_m is the additional modulation stiffness added by the magnet and coil interaction. The spring stiffness can be decomposed in the generalized Floquet form,

$$\kappa(t) = \sum_{p=-1}^{1} \kappa_p e^{j\Omega t + \phi_p} \tag{1}$$

where $\kappa_{\pm 1}$ equals to $0.5\kappa_m$. At low frequency, the generalized Floquet form of flexural wave displacement in a thin plate can be expressed as the sum of harmonic propagation and evanescent modes[15],

$$w = \sum_{n=-N}^{N} \left(A_n e^{-jkx} + B_n e^{jkx} + a_n e^{-kx} + b_n e^{kx}\right) e^{j(\omega + n\Omega)t} \tag{2}$$

where k is the wave number, and ω is the operational angular frequency. The displacement of the mass in the resonator is,

$$w^m(t) = \sum_{n=-N}^{N} w_n^m e^{j(\omega + n\Omega)t} \tag{3}$$

The conditions of continuity on the displacement w, slope φ, moment balance M, and beam shear force balance V, apply in the waveguide[25] at $x = 0$,

$$\begin{cases} w^+ - w^- = 0 \\ \varphi^+ - \varphi^- = 0 \\ M^+ - M^- = 0 \\ V^+ - V^- = F \end{cases} \tag{4}$$

The positive and negative signs mean right and left of the position $x = 0$ of the beam. And the slope, the moment and shear force are,

$$\begin{cases} \varphi = \dfrac{\partial w}{\partial x} \\ M = EI \dfrac{\partial^2 w}{\partial x^2} \\ V = -EI \dfrac{\partial^3 w}{\partial x^3} \end{cases} \tag{5}$$

where $I = h^3/12(1 - \upsilon^2)$ is the section moment of inertia, and E and υ are the Young's modulus and Poisson's ratio of the waveguide, respectively.

At $x = 0$, $F(0) = (w^+(0) - w^m)\kappa(t)$, and an extra equation of the force balance on the mass exists,

$$m \frac{\partial^2 w^m}{\partial t^2} = F(0) \tag{6}$$

The dispersion relation is known as $k = (EI/\rho h\omega^2)^{-\frac{1}{4}}$, where ρ is the density of the waveguide. We insert Eqs (1) to (3) into Eqs (4) to (6); and by considering a finite number N of plane waves and by eliminating $\boldsymbol{w}^{m,N}$, we are able to obtain the transfer matrix $\boldsymbol{M}$ of dimension $4(2N + 1)$,

$$\begin{bmatrix} \boldsymbol{A}^{+,N} \\ \boldsymbol{B}^{+,N} \\ \boldsymbol{a}^{+,N} \\ \boldsymbol{b}^{+,N} \end{bmatrix} = \boldsymbol{M} \begin{bmatrix} \boldsymbol{A}^{-,N} \\ \boldsymbol{B}^{-,N} \\ \boldsymbol{a}^{-,N} \\ \boldsymbol{b}^{-,N} \end{bmatrix} \tag{7}$$

where $\boldsymbol{A}^{+,N}$, $\boldsymbol{B}^{+,N}$, $\boldsymbol{a}^{+,N}$, $\boldsymbol{b}^{+,N}$, $\boldsymbol{A}^{-,N}$, $\boldsymbol{B}^{-,N}$, $\boldsymbol{a}^{-,N}$ and $\boldsymbol{b}^{-,N}$ are of the form $\boldsymbol{X}^{s,N} = \langle X_{-N}^{s}, \dots, X_{0}^{s}, \dots, X_{+N}^{s} \rangle^{T}$ where $\boldsymbol{X}$ can be either $\boldsymbol{A}$, $\boldsymbol{B}$, $\boldsymbol{a}$ or $\boldsymbol{b}$ and s takes either the sign "−" or "+", and $\boldsymbol{w}^{m,N} = \langle w_{-N}^{m}, \dots, w_{0}^{m}, \dots, w_{+N}^{m} \rangle^{T}$. This transfer matrix $\boldsymbol{M}$ can be converted to the scattering matrix $\boldsymbol{S}$

$$\begin{bmatrix} \boldsymbol{A}^{+,N} \\ \boldsymbol{a}^{+,N} \\ \boldsymbol{B}^{-,N} \\ \boldsymbol{b}^{-,N} \end{bmatrix} = \boldsymbol{S} \begin{bmatrix} \boldsymbol{A}^{-,N} \\ \boldsymbol{a}^{-,N} \\ \boldsymbol{B}^{+,N} \\ \boldsymbol{b}^{+,N} \end{bmatrix} \tag{8}$$

The incident, reflected and transmitted wavefields are $w_i = \sum_{n=-N}^{N} \left(A_{\mathrm{n}}^{-} e^{-jkx}\right) e^{j(\omega+n\Omega)t}$, $w_r = \sum_{n=-N}^{N} \left(B_{\mathrm{n}}^{-} e^{jkx} + b_{\mathrm{n}}^{-} e^{kx}\right) e^{j(\omega+n\Omega)t}$, and $w_t = \sum_{n=-N}^{N} \left(A_{\mathrm{n}}^{+} e^{-jkx} + a_{\mathrm{n}}^{+} e^{-kx}\right) e^{j(\omega+n\Omega)t}$, respectively. With a given w_i, w_r and w_t can be calculated. If the points of the measurement are far enough from the two resonators system (one wavelength away), the evanescent terms in the w_r and w_t can be ignored.

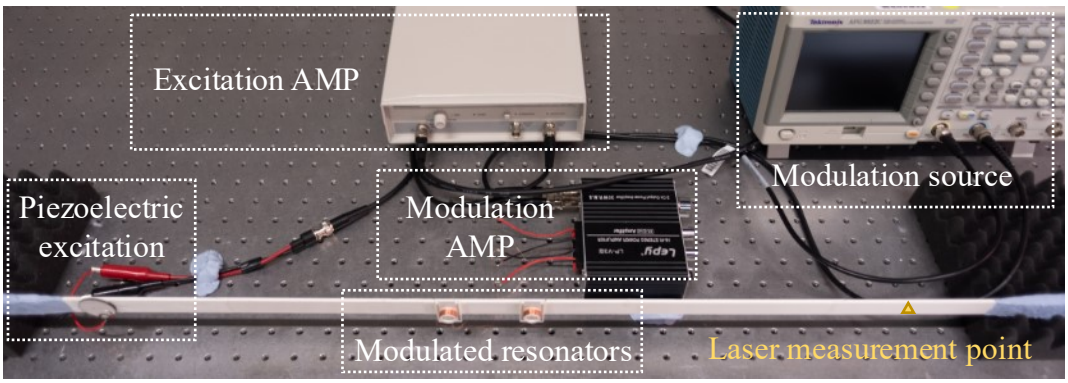

FIG. 2. Experimental platform for flexural wave transmission. AMP: amplifier.

Figure 2 shows the experimental setup of the system. We first have constructed a beam waveguide by 3D printing using PLA material and the beam width and thickness are $d = 20$ mm and $h = 3$ mm, respectively. Damping adhesives were sticked on the two extreme boundaries of the beam to eliminate the flexural wave reflections at low frequency, and ensure weak reflection above 120 Hz. The whole length of the beam is over 3 m, and the usable length of this beam is approximately 0.8 m, about 3 wavelengths at 126 Hz. A large circular piezoelectric patch with a radius of 15 mm was used as an excitation source, which prevents the appearance of torsional modes on the beam. An additional amplifier was connected to the piezoelectric patch to perform a strong excitation while reducing the influence of the

background noise. The manually mounted resonators were glued on the beam. The two-channel external source generator and the two-channel amplifier were connected to the coils to drive the temporal modulation. The amplifier was indispensable because the electrical impedance of the coil at 20 Hz is about 15 Ohm and the power consumption of a single coil is up to 3.4 W (with an effective current of 0.46 A). The necessary current to reach a required κ_m was estimated via finite element simulation, and the real current needed in the experiment was higher than the simulation results due to the fabrication imperfections of coils (see **Supplementary information**). The magnet is rigidly bonded to the base of the cantilever, which is glued on the beam (**Fig.1(d)**), and the measurement was performed via laser vibrometer. The coil is glued on the skeleton of the cantilever, which enables the out-of-plane movement. The mass of the coil is 2.5 g, the frequency of the first resonance mode is about 115 Hz, and the distance between the centers of the two resonators is 70 mm. The spring stiffness κ_0 under 20°C is approximately 1600 N/m (See **Supplementary information** for the details of evaluations of the effective stiffness κ_0 and the effective mass m). We optimized the effect of nonreciprocity upon the modulation frequency Ω, the modulation strength κ_m, and the distance between the two resonators l using genetic algorithm. The magnet and the coil should be strictly coaxial and concentric. If not, the AC itself could become an excitation source at the AC frequency Ω. In this situation, high noise at the harmonics of the AC frequency would be generated.

In the experimental setup, the power consumption leads to a rapid heating of the resonators which may at some points makes the PLA lose its original rigidity and effects the resonance mechanism and the measurements. To reduce the heating effect, we adopted a low effective current 0.46 A and shortened the power-on time of the coils. With this current, the modulation strength κ_m we can reach is approximately 200 N/m. The Fast Fourier Transform (FFT) resolution of the laser vibrometer was set to 1 Hz, and the measurements were performed on one point on the beam so that each measurement can be done in 1 s. Then, the power-on time was controlled by activating and disactivating the output of the modulation source generator. The modulation amplifier was always on to prevent power-on sonic boom. The excitation source was also always on to reduce the influence of the astable state. The precise output phase setting is available on our modulation generator, so the phase shift was realized by applying different initial phases on the outputs of different channels. Further, to inverse the direction of propagation, it is sufficient to inverse the phase shift of the two output channels. The frequency

of AC, i.e. the modulation frequency Ω, is 20 Hz. The phase shift between the two ACs is 90° or −90°. At each frequency, we performed 5 measurements in each propagation direction.

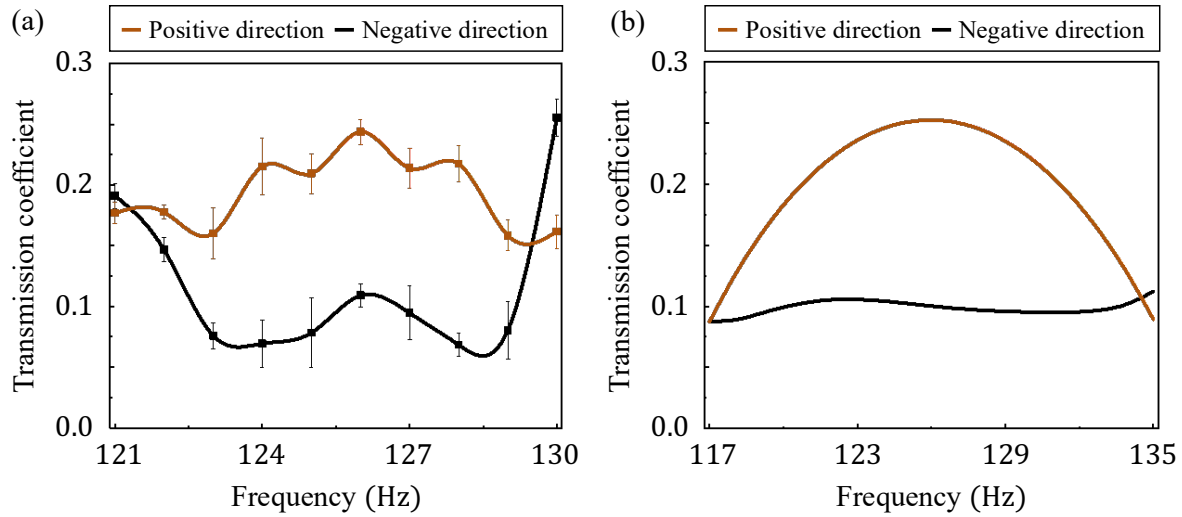

FIG. 3. (a) Results of the transmission measurements from 121Hz to 130Hz with error bars, normalized by the results of the bare beam (without resonators). The positive direction means the initial phase of current of the coil close to the piezoelectric excitation is 90°, while that close to the laser measurement point is 0°. The negative direction means the former is −90°, while the latter is 0°. (b) Analytical transmission coefficient A_0^+ in the frequency domain.

Fig. 3(a) shows the results of the measured transmission with error bars, which is normalized by the result of the bare beam (without the resonators). The curve is obtained by an interpolation function over the points of measurement. **Fig. 3(b)** shows the corresponding theoretical results, where the effective resonance frequency of the structure is a bit lowered to 113 Hz due to heating effect (The spring stiffness is respectively reduced to about 1500 N/m) (see **Supplementary information** for the detailed parameters we adopted for the theoretical model). We can clearly evidence the nonreciprocal wave transmission for flexural waves with an acceptable agreement observed between theory and experiment. The bandwidth of the measurement result is however relatively different from that of the theory because of the approximations made in modeling the resonators. The error bars indicate the stability and reproducibility of the measured nonreciprocal transmission in our system.

To better understand the mechanism of nonreciprocity in our structure, we have analyzed the mechanical energy of the transmitted and reflected waves, as well as in the resonators using numerical approaches for the case with time modulated effective stiffness. To conduct the

transmission simulation using finite element simulation, the reflections of flexural waves at the boundaries of the beam are suppressed using the damping layer method[26]. An example evaluation of the reflection and transmission coefficients for an incident harmonic wave at 126 Hz is shown in **Fig. S3** in the **Supplementary information**. Frequency conversion is depicted with the appearance of high order waves at frequencies $126\ \text{Hz} + n\Omega$ where $n = \pm 2, \pm 1$.

The mechanical energy in the flexural wave on the plate can be calculated[27],

$$E_b = \omega E I k^3 |\bar{X}|^2 , \tag{9}$$

where $|\bar{X}|$ is the amplitude of the flexural wave. The mechanical energy in the resonator can also be calculated using the formula,

$$E_k = \frac{1}{2} m(\omega |w^m|)^2 \tag{10}$$

$$E_p = \int_0^{T_M} \frac{1}{2} [k_0 + k_m \cos(\Omega t)] |w^m|^2 dt \tag{11}$$

where E_k is the kinetic energy of the mass, E_p is the potential energy of the spring, and $T_M = 2\pi/\Omega$ is the cycle of the temporal modulation. **Fig. 4** exhibits the stacked area charts of the mechanical energy of the system in both propagation directions for incident harmonic waves with frequencies between 117 and 135 Hz. The chart represents the calculated energy for the transmission (green) and reflection (pink) waves in the plate, the energy stored in the resonators (yellow), and the sum of the energies carried by the high order waves at frequencies $\omega + n\Omega$ where $n = \pm 2, \pm 1$ for the transmitted (orange) and reflected waves (blue), as well as in the resonators (purple), all normalized by incident wave energy. Considerable frequency conversions appear in this time-modulated system, which is the principal incentive for the nonreciprocity in our structure. We observe that the low transmitted energy (green) of the fundamental mode (0th order) in the negative direction is attributed to frequency conversion in the transmitted (orange) and reflected waves (blue). Another observation is that the total energy in our structure surpasses the input energy from incident wave due to the input energy from active time modulation.

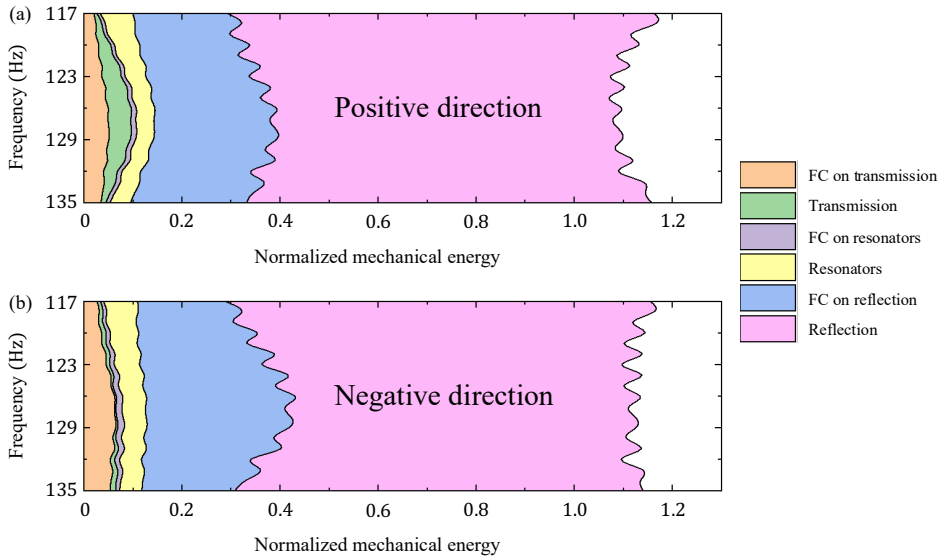

FIG. 4. Stacked area chart of global mechanical energy distribution for positive (a) and negative (b) directions calculated using FE simulation at various incident frequencies. FC: frequency conversion. Here we represent the mechanical energy for the transmitted (green) and reflected (pink) fundamental modes (0th order) in the plate, the energy stored in the resonators (yellow), and the sum of the energies carried by the high order waves at frequencies $\omega + n\Omega$ where $n = \pm 2;\ \pm 1$ for the transmitted (orange) and reflected waves (blue), as well as in the resonators (purple), all normalized by incident wave energy.

In conclusion, we have introduced in this work a compact time-modulated mechanical bi-resonators system to achieve nonreciprocal flexural wave transmission at low frequency. The resonators were designed with a vibrating cantilever with magnetically coupled coils and magnets. The temporal modulation of the effective stiffness of each resonator was realized by an AC applied to the coil which couples to the fixed magnets via the varying magnetic field. The dimension of this device is less than $1/3$ wavelength. A physical realization of such a system based on coil-cantilever-magnet resonators has been experimentally conducted. The obtained measurements have evidenced high nonreciprocal flexural waves propagation with results that agree well with our simplified analytical predictions. Our concept provides a promising perspective on the design of compact nonreciprocal metamaterials that can integrate flexural waveguiding systems for smart wave control in phononic communication devices.

Supplementary material

See supplementary material for all the details regarding the manuscript.

Acknowledgements

This work is supported by the Air Force Office of Scientific Research under award number FA9550-18-1-7021, and by la Région Grand Est.

Author declarations

Conflict of interest

The authors have no conflicts to disclose.

Data availability

The data that support the findings of this study are available within the article and its supplementary material.

References

[1] H. Nassar, B. Yousefzadeh, R. Fleury, M. Ruzzene, A. Alù, C. Daraio, A.N. Norris, G. Huang, and M.R. Haberman, Nat. Rev. Mater. **5**, 667 (2020).

[2] D.L. Sounas and A. Alù, Nature Photon. **11**, 774 (2017).

[3] C. Caloz, A. Alù, S. Tretyakov, D. Sounas, K. Achouri, and Z.-L. Deck-Léger, Phys. Rev. Applied **10**, 047001 (2018).

[4] J. Kim, M.C. Kuzyk, K. Han, H. Wang, and G. Bahl, Nature Phys. **11**, 275 (2015).

[5] R. Fleury, D. Sounas, M.R. Haberman and A. Alù, Acoust. Today **11**, 14 (2015).

[6] R. Fleury, D.L. Sounas, C.F. Sieck, M.R. Haberman, and A. Alù, Science **343**, 516 (2014).

[7] L. Fan and J. Mei, Phys. Rev. Applied **15**, 064002 (2021).

[8] Y. Zhu, L. Cao, A. Merkel, S.-W. Fan, B. Vincent, and B. Assouar, Nat Commun. **12**, 7089 (2021).

[9] D.L. Sounas, C. Caloz, and A. Alù, Nat Commun. **4**, 2407 (2013).

[10] T. Kodera, D.L. Sounas, and C. Caloz, Appl. Phys. Lett. **99**, 031114 (2011).

[11] A. Oliner and A. Hessel, IRE Trans. Antennas Propag. **7**, 201 (1959).

[12] E.S. Cassedy and A.A. Oliner, Proc. IEEE **51**, 1342 (1963).

[13] E.S. Cassedy, Proc. Inst. Electr. Eng. **112**, 269 (1965).

[14] Y. Wang, B. Yousefzadeh, H. Chen, H. Nassar, G. Huang, and C. Daraio, Phys. Rev. Lett. **121**, 194301 (2018).

[15] Y. Chen, X. Li, H. Nassar, A.N. Norris, C. Daraio, and G. Huang, Phys. Rev. Applied **11**, 064052 (2019).

[16] B.M. Goldsberry, S.P. Wallen, and M.R. Haberman, J. Acoust. Soc. Am. **146**, 782 (2019).

[17] J. Marconi, E. Riva, M. Di Ronco, G. Cazzulani, F. Braghin, and M. Ruzzene, Phys. Rev. Applied **13**, 031001 (2020).

[18] G. Trainiti, Y. Xia, J. Marconi, G. Cazzulani, A. Erturk, and M. Ruzzene, Phys. Rev. Lett. **122**, 124301 (2019).

[19] C. Sugino, M. Ruzzene, and A. Erturk, Phys. Rev. B **102**, 014304 (2020).

[20] M.A. Attarzadeh, J. Callanan, and M. Nouh, Phys. Rev. Applied **13**, 021001 (2020).

[21] S. Wan, L. Cao, Y. Zhu, M. Oudich, and B. Assouar, Phys. Rev. Applied **16**, 064061 (2021).

[22] C. Shen, J. Li, Z. Jia, Y. Xie, and S.A. Cummer, Phys. Rev. B **99**, 134306 (2019).

[23] C. Shen, X. Zhu, J. Li, and S.A. Cummer, Phys. Rev. B **100**, 054302 (2019).

[24] X. Zhu, J. Li, C. Shen, X. Peng, A. Song, L. Li, and S.A. Cummer, Appl. Phys. Lett. **116**, 034101 (2020).

[25] L. Cao, Z. Yang, Y. Xu, Z. Chen, Y. Zhu, S.-W. Fan, K. Donda, B. Vincent, and B. Assouar, Mech. Syst. Signal. Process. **146**, 107035 (2021).

[26] Y. Shen and V. Giurgiutiu, Wave Motion **58**, 22 (2015).

[27] L. Cao, Y. Zhu, Y. Xu, S.-W. Fan, Z. Yang, and B. Assouar, J. Mech. Phys. Solids **154**, 104502 (2021).